Title: A Study of a Turbulent Jet Ignition System Fueled with Iso-octane: Pressure Trace Analysis and Combustion Visualization

Keywords: turbulent jet ignition; combustion visualization; ignition enhancement; controlled autoignition

Authors and Affiliations:

Gerald Gentz [a], Masumeh Gholamisheeri [a], Elisa Toulson [a]

a. Department of Mechanical Engineering, Michigan State University, East Lansing, MI 48824, USA

Corresponding author's contact information:
1497 Engineering Research CT
East Lansing, MI 48823
USA
Fax: 517-432-3341
Email: toulson@msu.edu

List of figures and captions

List of tables

Abstract

Turbulent Jet Ignition is an advanced pre-chamber ignition enhancement technique for spark ignition engines that uses a discharging jet of hot combusting gases to initiate main chamber combustion. The jet acts as a distributed ignition source, leading to fast burn rates and increased combustion stability. Experiments were performed in an optically accessible rapid compression machine using liquid iso-octane to study the effects of auxiliary fuel injection and ignition distribution due to nozzle geometry. A custom low-flow fuel injector was used to overcome previous limitations of using liquid fuel in the pre-chamber. Jet induced autoignition behavior was also studied in depth by considering high-speed images, pressure traces, and pressure derivative data.

1. Introduction

Major initiatives are underway in the United States to improve combustion efficiency, reduce emissions and enhance energy security by decreasing reliance on foreign energy sources. Extensive research on advanced ignition engines that operate lean or highly diluted through low temperature combustion (LTC) is currently of interest as this provides a means to reduce NOx emissions while maintaining fuel efficiency [1-5]. However, the combustion of lean and highly dilute mixtures is challenging to implement since as the mixture becomes increasing lean, the burning speed becomes much slower and combustion starts to become unstable [6]. In this case, ignition enhancement allows for faster burning rates and increased stability either by increasing the ignition energy supplied, and/or distributing the ignition source over many ignition sites [6-8]. Turbulent jet ignition (TJI) is one such advanced ignition enhancement technique for spark ignition engines, where a jet of hot combusting gases is used as the ignition source. With TJI, combustion is initiated in a pre-chamber by conventional spark ignition, generating a rapid increase in temperature and pressure that force combusting gases out of the pre-chamber though one or more small orifices. Heat and radical species are distributed throughout the discharging jet volume, and act as the ignition source for the main chamber charge as the unburned mixture becomes entrained. This distributed ignition effect leads to fast burn rates and increased combustion stability [8].

The concept of jet ignition was first introduced in the late 1950's in the Soviet Union under the direction of Nikolai Semenov, who is famous for his contributions to chain reaction theory [9, 10]. Lev Gussak was one of the researchers working with Semenov to develop the first jet ignition engine. They gave the ignition concept the name LAG (Lavinaia Aktivatsia Gorenia) which translates to "Avalanche Activated Combustion" [8-13]. LAG is essentially a divided-chamber stratified-charge ignition concept that uses a chemically reacting jet of fuel-rich combustion products to initiate combustion in ultra-lean mixtures. The advantages to this combustion process include limiting the occurrence of engine knock, reducing the required fuel octane number, increasing combustion stability for lean mixtures, lowering specific fuel consumption, and decreased formation of pollutants [11]. In the pioneering experimental work on the LAG process performed by Gussak in a pre-chamber engine [11, 12], a rich mixture (λ=0.5) was delivered to the pre-chamber via a cam actuated injector, and a lean mixture of λ=2.0 was able to be ignited within the cylinder. λ is defined as the air-fuel equivalence ratio, or relative air-fuel ratio. Through extensive experiments, Gussak found that a pre-chamber volume 2-3% of the clearance volume and a total orifice area of 0.03-0.04 cm^2 per 1 cm^3 of pre-chamber volume optimized the LAG process.

Later, Oppenheim et al. [14-16] at the University of California, Berkeley developed a similar ignition concept termed Jet Plume Injection and Combustion (JPIC). The JPIC igniter is essentially a miniaturized version of the valve-operated LAG combustion system that can be installed into an engine similar to a direct injector [8, 15]. Ultra-lean mixtures of λ=2.22 could be ignited by JPIC, while the lean limit for spark ignition was determined to be λ=1.53. For nozzle diameters of 2.5 mm, 4 mm, and 6 mm, combustion performance was evaluated based on parameters of the pressure traces such as maximum pressure, and the slope of the pressure curves. Murase and Hanada [17-19], also performed extensive research on the JPIC ignition concept. In one study [19], jet ignition was used as a trigger to control the start of Homogenous Charge Compression Ignition (HCCI), with direct visualization of the jet discharging and initiating combustion.

In the 1990's, at the University of Melbourne, Watson et al. [20-22] developed a pre-chamber ignition concept named Hydrogen Assisted Jet Ignition (HAJI). HAJI is similar to the other pre-chamber jet ignition concepts mentioned in this paper; the hardware consists of a small pre-chamber and orifices, spark plug, and pre-chamber direct injector. As the name suggests, hydrogen is used as the pre-chamber fuel. Toulson et al. performed a study of the HAJI system in a single cylinder research engine with Liquefied Petroleum Gas (LPG) as an alternative pre-chamber fuel, with the LPG having a composition of 95% propane and 5% butane [21]. Main chamber fuels tested were both LPG and gasoline. In this study, the experimental lean limit was defined to be when the coefficient of variation of the indicated mean effective pressure exceeded 10%. As a baseline, spark ignition was determined to have a lean limit of 1.25. Using hydrogen as the pre-chamber fuel was shown to extend the lean limit the furthest to λ=2.6 with gasoline as the main-chamber fuel and λ=2.5 for the case when LPG was used as the main-chamber fuel.

Using LPG as the pre-chamber fuel also showed a significant extension of the lean limit to λ=2.35 for both LPG and gasoline as main chamber fuels. Analysis of the exhaust indicated that when LPG was used as the main-chamber fuel, the NOx emissions were reduced. Furthermore, mass burn rate calculations derived from the pressure traces showed the effect of the different pre-chamber and main chamber fuel combinations.

TJI is a further refinement of the jet ignition concept for direct application to standard spark ignition engines. Attard et al. performed extensive engine studies of TJI [23-29], including a visualization study of TJI in a single cylinder optical engine using natural gas at several air to fuel ratios and engine speeds [30], as well as demonstrating successfully that vaporized gasoline is a viable pre-chamber fuel [28].

The work of previous authors includes testing various pre-chamber fuels and fueling strategies. Using a single fuel source in an engine is preferable, with a liquid gasoline system being the most convenient to implement into existing spark ignition engines that already operate using liquid gasoline as the primary fuel. However, liquid gasoline pre-chamber fueling systems in the literature exhibit diminished performance due to poor mixture preparation caused by limitations of the injector hardware [25].

When using different fuels, the physics that occur during jet ignition may change due to changes in the thermochemistry. For instance, Murase and Hanada studied jet ignition using n-butane mixtures in a rapid compression machine and found that jet ignition triggered autoignition of the mixtures [19]. By analyzing the pressure traces and rate of pressure rise, along with high-speed imaging, the effect of nozzle diameter and ignition timing were investigated. Two different single orifice nozzles were used with diameters of 2.5 mm and 4.0 mm, and the jet behavior was found to change with the orifice geometry and stoichiometric conditions [19].

In the current work a TJI system incorporating a custom “low flow” pre-chamber fuel injector was used to overcome the limitations of using liquid fuel as the pre-chamber fuel. Experiments were performed in an optically accessible rapid compression machine in order to characterize the TJI performance with varying nozzle geometry and proportion of auxiliary injected mass using iso-octane. The nozzles were chosen to have a single orifice and dual orifice geometry with equivalent cross-sectional flow area to study the effects of ignition distribution. In the experiments, it was discovered that the jets were inducing autoignition of the unburned mixture similar to what was observed by Murase and Hanada in their study [19]. In the literature, autoignition is not a well-studied problem with respect to jet ignition. Therefore, the TJI induced autoignition is investigated in detail by analyzing the high-speed images and derivatives of the pressure curves.

2. Experimental Set-up

The Rapid Compression Machine (RCM) used for the experiments is shown in Figure 1. The RCM operates using three pistons (combustion, hydraulic, and pneumatic) coupled together with two shafts such that any motion from one of the pistons is transferred to the others. During operation, high-pressure oil in the hydraulic reservoir provides a holding force for the system, while pressurized air acting on the pneumatic piston serves as the driving force. When triggered, a solenoid valve vents the high-pressure oil in the hydraulic reservoir. No longer restrained, the piston system is driven forward until the hydraulic piston reaches the end of the reservoir where it is stopped due to mechanical interference. By introducing shims in the back flange of the hydraulic chamber, the stroke length may be adjusted, which allows the RCM compression ratio to be variable.

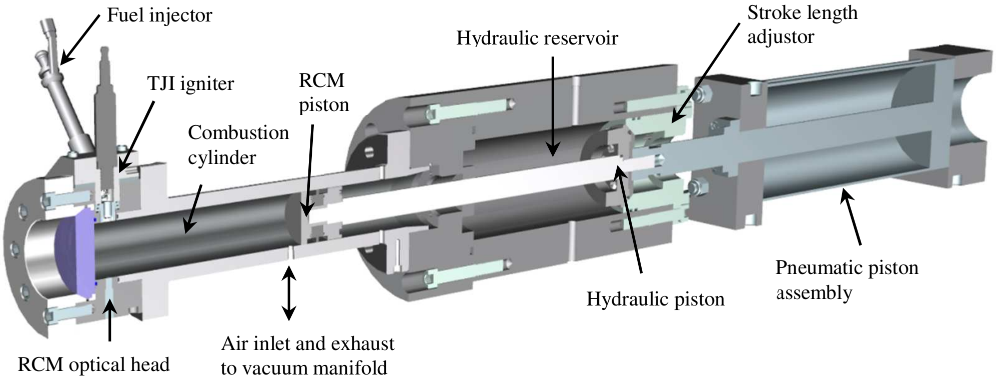

Figure 1. RCM illustration showing the location of the TJI igniter with the piston at BDC

The motion of the RCM piston compresses the charge of fuel and air in the combustion cylinder to an elevated temperature and pressure suitable for combustion, which occurs at constant volume when the piston has reached the end of its stroke. The RCM utilizes a single stroke, and the piston remains at the Top Dead Center (TDC) position until it is returned to the starting position after the test. Figure 2 shows a view of the RCM optical head and TJI Igniter when the piston has reached TDC.

Figure 2 shows an illustration of the TJI igniter installed on the top of the RCM optical head. A Kistler spark plug with incorporated pressure sensor threads into the pre-chamber adapter, and there are two ports in the pre-chamber adapter body for fuel injectors to be installed. To complete the pre-chamber assembly, a nozzle with the desired geometry (with one or more orifices) is threaded into the bottom of the pre-chamber. When these components are assembled together, the pre-chamber geometry is defined, with the main chamber connected to the pre-chamber via the nozzle orifices.

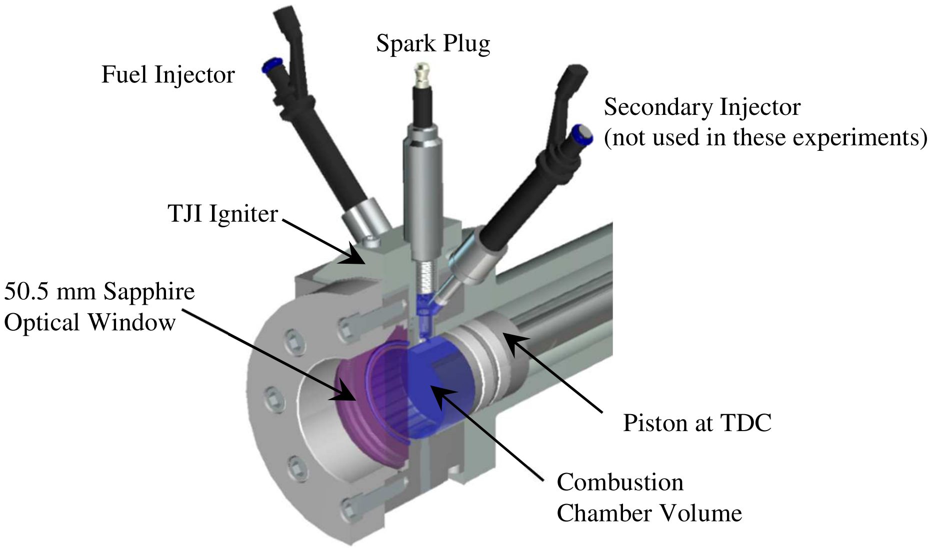

Figure 2. Illustration of the RCM Optical and TJI igniter used, with the RCM piston at TDC.

The RCM optical head and cylinder are pre-heated using band heaters, which are controlled by a LabVIEW program. LabVIEW is also used for signal generation (ignition coil dwell signal, fuel and air injection pulses) and data acquisition (control signals, pre-chamber pressure, and main chamber pressure).

Prior to performing a test the combustion chamber is evacuated of all gasses using a vacuum pump through a small port at the bottom of the combustion cylinder. To prepare the initial charge of fuel and air, gasoline is pulsed through the pre-chamber fuel injector into the evacuated cylinder. Since the cylinder pressure is below the vapor pressure of the fuel, the fuel is vaporized and occupies the entire combustion chamber volume (main chamber and pre-chamber).

An absolute pressure transducer is installed onto a small manifold that is connected to the inlet port that allows the cylinder pressure to be measured, thus providing the partial pressure of the gasoline. For the chosen stoichiometry, the partial pressure of air can then be calculated and introduced to the cylinder via the inlet port by using a metering valve connected to a compressed gas cylinder. After the addition of air, the inlet valve is closed and the hydraulic reservoir is pressurized, followed by pressurization of the pneumatic piston. Upon triggering, a solenoid valve is actuated and the high pressure in the hydraulic reservoir vents, which allows the pneumatic piston to drive the coupled piston assembly forward, starting the piston motion. For auxiliary fueled cases, fuel is injected into the pre-chamber early in the compression stroke. The global (initial charge + auxiliary fuel) air-fuel equivalence ratio for the experiments here was held constant at 3.0. The typical mixture preparation time was approximately 3 minutes, which was determined to be an adequate time for pre-mixing. Experiments were performed for 3, 5, 10, and 20 minutes of pre-mixing time, with no discernable difference in the pressure traces or optical images.

Table 1 provides the different injector pulse widths used and the corresponding stoichiometric conditions. The pre-chamber λ is estimated by assuming that no fuel or air is displaced into the main chamber during the fuel injection event, since injection occurs during the compression stroke and fluid motion should be into the pre-chamber. The mass fraction m_i is also given, which is the ratio of the injected fuel mass to the total mass.

Table 1. Testing conditions for different auxiliary fuel injection pulse widths

PW (ms)	λ_{global}	$\lambda_{main\ chamber}$	$\lambda_{pre\text{-}chamber}$	m_i
0.00	3.0	3.0	3.0	0.0 %
0.50	3.0	3.02	2.60	0.7 %
0.75	3.0	3.15	1.25	6.6 %
1.00	3.0	3.30	1.06	8.6 %
1.25	3.0	3.35	0.93	10.7 %

The entire bore of the RCM cylinder is optically accessible through a 50.75 mm sapphire window. A Photron SA4 high-speed color camera equipped with a Nikon 50 mm f/1.2 objective lens is used to perform combustion visualization. An overview of the experimental setup can be found in Table 2. Further details regarding the experimental setup can be found in [31, 32].

Table 2. Overview of RCM experimental set-up

Cylinder Wall Temperature	120° C
Compression Ratio used	11.2
Cylinder Capacity	564.4 cm^3
Clearance Volume	50.63 cm^3
Piston Stroke Length	254 mm
Cylinder Bore	50.5 mm
Compressed pressures at TDC	2000 kPa
Main chamber fuel used	Iso-octane
Auxiliary fuel	Iso-octane
Auxiliary fuel injector	Bosch Direct Injector (proprietary "low flow" design)
TJI pre-chamber volume	2.51 cm^3
Nozzle Orifice Diameters	D= 2x 2.26 mm, D=1x 3.16 mm
Orifice length	3.0 mm
Electrical Ignition System	Conventional inductive discharge
Power Supply Voltage	13.5 V
Ignition Coil Dwell Time	5 ms
Spark Plug and Pre-Chamber Pressure Sensor	Kistler Type: 6117BFD17
Main chamber pressure sensor	Kistler Type: 6125C
High Speed Camera	Photron SA4
Objective lens	Nikon 50 mm f/1.2

3. Results and Discussion

Experiments were performed to determine the effect of varying the amount of auxiliary fuel mass and nozzle geometry. The single orifice and dual orifice nozzle were designed to have nearly equivalent cross sectional area, with dimensions of D=1x 3.16 mm and D=2x 2.26 mm, respectively, with slight differences in the area due to selecting the nearest drill size during machining. As a baseline, tests were first performed with no auxiliary fueling. For the auxiliary fueled cases injector pulse widths 0.5 ms, 0.75 ms, 1.0 ms, and 1.25 ms were used, corresponding to increasing quantities of injected mass. The global air-fuel equivalence ratio is kept constant at λ=3, thus for increasing amounts of auxiliary fuel mass, less fuel is present in the initial mixture in order to keep the total amount constant. Each experiment was performed five times to obtain some idea of the combustion stability and variability of the data. The experimental pressure traces for both nozzle geometries are shown in Figure 3, with the dual orifice results presented on the left, and the single orifice results on the right.

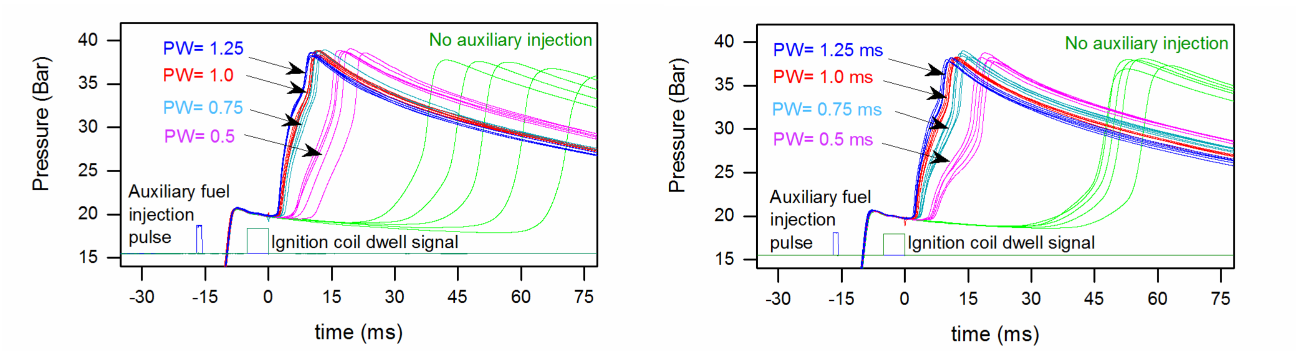

Figure 3: Experimental pressure traces for dual orifice (left) and single orifice (right) nozzle geometries

The timing of the auxiliary fuel injection event was set to be early in the compression stroke, about 10 ms before the end of compression and was held constant for each test.

Likewise, the spark timing was also constant for each test and occurred 7 ms after TDC (the spark occurs on the falling edge of the ignition coil dwell signal). In the figures, the time datum is chosen so that the time equals zero at the spark event. From the pressure traces, it can be seen that for increasing pulse widths, i.e. higher ratios of injected fuel mass, the combustion stability improves and the overall ignition delay is shortened. Another interesting feature that is apparent is that the two nozzles appear to produce different pressure profiles at the various pulse width conditions. Differences include the amount of variation in the curves, as well as differences in the general shape of the curves with inflection points occurring at different locations.

To compare between the two different orifice geometries used, the average of the five experimental curves for each auxiliary fueled condition and nozzle are plotted together in Figure 4.

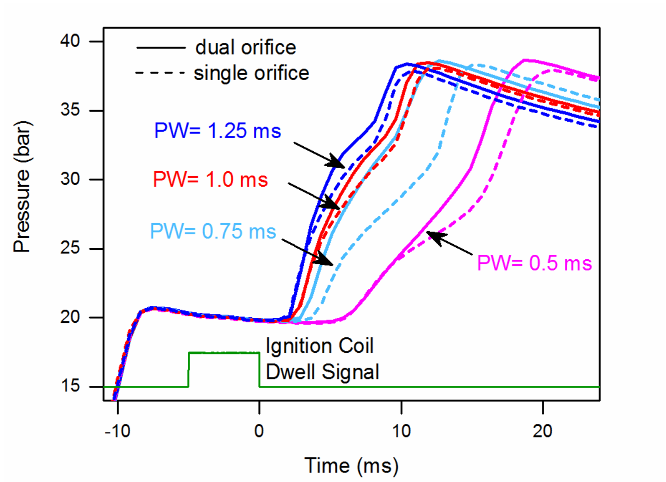

Figure 4: Average experimental pressure traces for dual orifice and single orifice nozzle geometries

In general, the pressure traces for the dual orifice tests precede the single orifice cases. With the exception of the 0.75 ms case, the pressure curves for both nozzles appear to match during the initial pressure rise, and then begin to deviate from each other. This implies that for the higher auxiliary injected mass, the conditions for ignition are stable and nearly the same, and that the differences in combustion are due to factors that occur later in the combustion process. However, this may be a somewhat misleading result in the case of PW= 0.5 ms, as there is considerable variation in the pressure traces, and just by chance the average pressure traces match initially (see Figure 3).

The ignition quality and speed of combustion can be determined quantitatively from the pressure traces by considering the duration of combustion. In previous RCM studies, the duration of 0%-10% of the pressure rise due to the combustion has been used to characterize the ignition stage, while the duration of 10%-90% of the pressure rise gives an indicator of how quickly the combustion of the overall charge occurs once ignition has been initiated [31]. Figure 5 shows a pressure diagram of a typical pressure trace, with annotations detailing the definition of these burn durations. Initially there is a pressure rise due to the piston motion. For auxiliary fueled cases, fuel is injected towards the beginning of the compression stroke. At the end of compression the piston has reached TDC and remains in that position until after the test is complete, creating a constant volume condition in the combustion chamber for the entire test. The spark in the pre-chamber is initiated shortly after TDC, with the time datum zero corresponding to the moment of the spark discharge event.

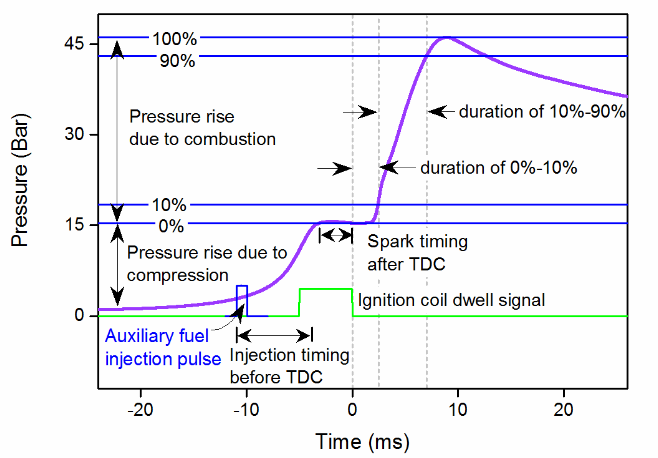

Figure 5. Typical pressure trace showing definition of 0%-10% and 10%-90% burn duration parameters

This produces a pressure rise strictly due to combustion, since the piston is stationary and the combustion chamber is at constant volume. The pressure reaches a maximum, and subsequently falls due to heat transfer to the surroundings. The pressure is then scaled so that 0% corresponds to the pressure at the time that the spark plug fires, and 100% corresponds to the maximum pressure achieved.

The mean 0%-10% and 10%-90% burn durations for the auxiliary fuel variation experiments are shown in Figure 6 for both nozzles, with the error bars representing the standard error of the mean.

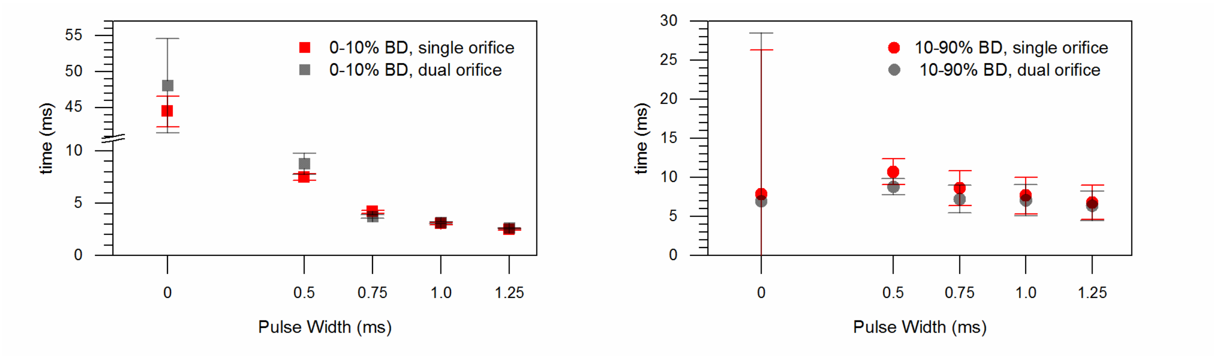

Figure 6. 0%-10% burn durations (left) and 10%-90% burn durations (right)

It can be seen that the 0%-10% burn duration for the non-auxiliary fueled case is much longer compared to the auxiliary fueled cases. The relatively large error bars also demonstrate the variability in the pressure traces as seen in Figure 3. These results indicate poor ignition quality due to the very lean mixture in the vicinity of the spark plug. For the non-auxiliary fueled case and for a pulse width of 0.5 ms, the single orifice has a faster 0%-10% burn duration than the dual orifice nozzle, while for pulse widths of 0.75 ms, the dual orifice nozzle has a faster 0%-10% burn duration. For pulse widths of 1.0 ms and 1.25 ms, the burn durations are the shortest and nearly identical for the two different orifices.

These results can be further interpreted by considering the physics that are occurring. The jet acts as a distributed ignition source, with the combusting jet either being channeled through a single orifice or being channeled through two orifices with an equivalent cross-sectional flow area. The dual jets will have a greater surface area, increasing the volume of colder unburned mixture that can be entrained, which decreases the bulk temperature of the jet in addition to the convective and radiative heat transfer losses that are also associated with an increased surface area. In addition, for the leaner cases, the adiabatic flame temperature is lower and the minimum ignition energy is higher. For these reasons, the jet that issues from the single orifice nozzle produces an ignition source that is more concentrated and able to reach the minimum ignition energy threshold more easily. Once the auxiliary fuel loading is increased, the mixture stoichiometry in the pre-chamber is closer to stoichiometric and is easily ignitable. With a lower minimum ignition energy threshold for these cases, both the single orifice and dual orifice jets produce ignition sources that reliably and rapidly initiate combustion in the main chamber.

From Figure 6 it can be seen that the 10%-90% burn durations for the non-auxiliary fueled cases are comparable to the auxiliary fueled cases, but with greater variability. Initially, the relatively fast burn duration for these cases was surprising since the ignition quality was poor as determined by the 0%-10% burn durations. Upon closer inspection of the pressure traces (Figure3) and the optical Images (Figure 7), it was determined that the jet discharge was inducing autoignition of the unburned charge in the main chamber. The mean 10%-90% burn duration is slightly shorter for the non-auxiliary fueled case compared to the auxiliary fueled case due to a larger proportion of the unburned charge undergoing autoignition, which increases the heat release rate. This causes the overall combustion duration to be shorter, but with combustion being less stable than the auxiliary fueled cases which have a smaller amount of end gas undergoing autoignition. This behavior is explained in more detail as the optical images are presented and further interpreted. It is important to note that when examining the raw pressure traces, there is no evidence of the high-frequency pressure oscillations that are associated with knocking combustion. This is likely because the pressure rise rates are not excessively high, the end-gas volume is small, and the overall lean conditions lead to lower temperatures and pressures than what would occur during stoichiometric combustion.

At a pulse-width of 0.5 ms the 10%-90% burn duration is a few milliseconds slower than the case without auxiliary fuel loading, but with dramatically improved stability apparent from the relatively small size of the error bars. As the injector pulse width is further increased, the 10%-90% burn duration becomes shorter indicating faster combustion overall. For all cases, the dual orifice jet results in a shorter 10%-90% burn duration due to the increase in surface area and the volume of entrained reactants.

Figure 7 shows the optical images obtained for the two different nozzle geometries for an auxiliary fueled condition using a 1 ms pulse width, and a non-auxiliary fueled condition for comparison. Images were selected so that similar features are shown in each frame i.e. the first set of images show the development of the jet, while the later frames show autoignition events. Due to these events occurring at different times, the time steps are indicated for each image sequence presented. The brightness and contrast for each image is enhanced using ImageJ, an image processing software available for download by the National Institutes of Health [33]. In addition, the auxiliary fueled cases and non-auxiliary fueled cases were captured at different frame rates. Although the luminosity intensity appears comparable for the images shown in Figure 7, the emission of light is orders of magnitude higher for the auxiliary injected cases taken at the faster frame rate than for the case without auxiliary fuel injection, which was taken at the slower frame rate.

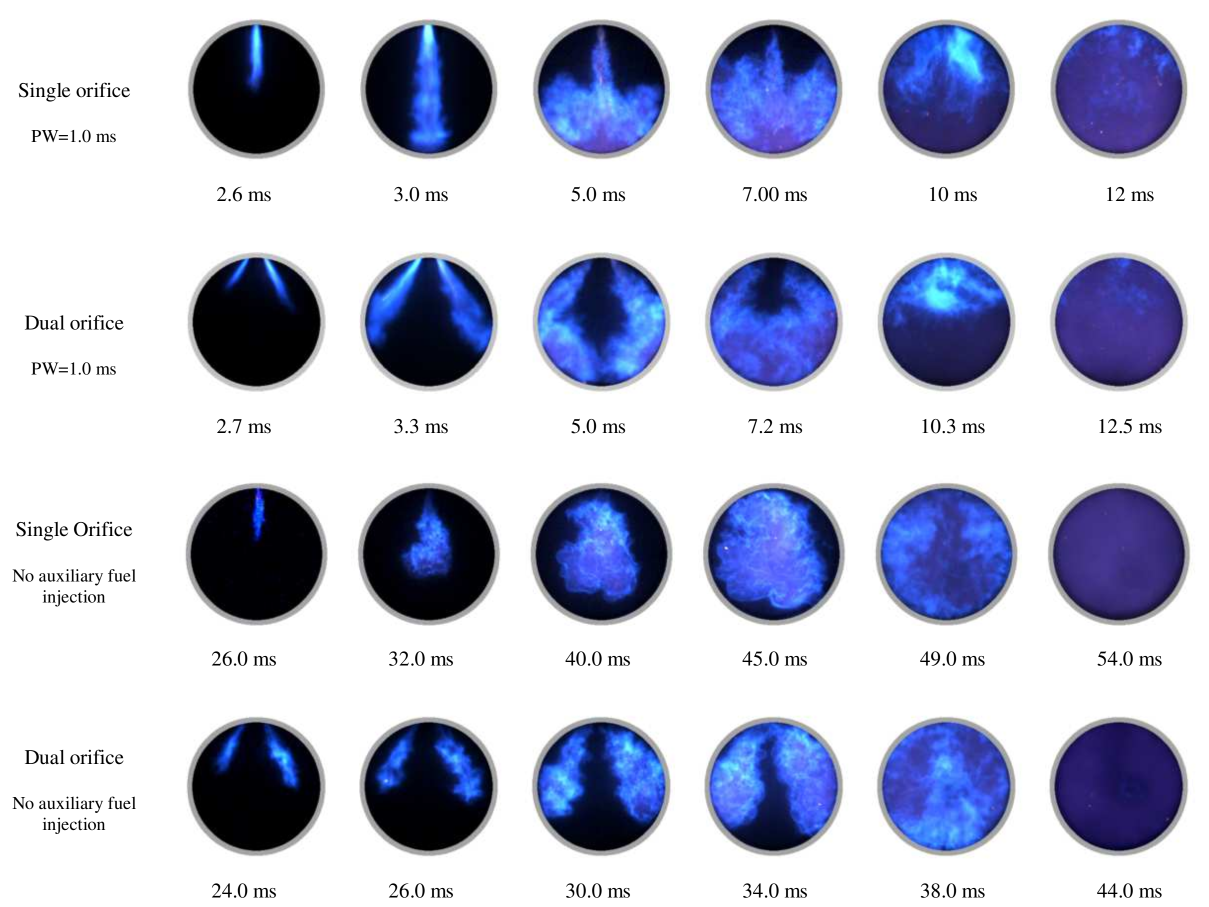

Figure 7. Combustion visualization of dual and single orifice TJI for non-auxiliary fueled jet ignition and jet ignition with auxiliary fuel injection (PW=1.0 ms)

For the auxiliary fueled jet ignition cases that are presented, there is stratification of the charge, with the pre-chamber becoming enriched and a leaner main chamber. The reacting jet discharges quickly, with a high momentum resulting in a narrow column of fluid that penetrates the chamber and reaches the end wall. For the jet issuing from the single orifice nozzle, a stagnation zone is created at the bottom of the cylinder and a wall jet is formed, where the fluid flow is bounded by the cylinder wall and directed upwards towards the unburned mixture. Combustion is enhanced by this fluid motion, and shortly thereafter the jet discharge event ends followed by a slower deflagration that continues to propagate. The end gas, which is defined as the remaining fuel and air mixture that has not been consumed, is being compressed by the flame front. Autoignition of the end gas then occurs, where the remaining fuel-air mixture is rapidly consumed. This is evident by the much brighter chemiluminesence of the reacting mixture compared to the region of burned gases, where the fuel and air has already been consumed by the jet. Furthermore, the duration of the autoignition event is very short and corresponds to the rapid rise in pressure as seen in the pressure traces in Figure 3.

For the auxiliary fueled dual orifice jet, the shape is also narrow initially, but with this nozzle the two jets impinge on the side of the cylinder creating a fluid motion that directs the hot jets toward the unburned mixture at the bottom of the cylinder. When the two jets meet, they create an opposed jet flow, enhancing mixing and entrainment of the unburned mixture. Combustion occurs within this flow field, and a flame front propagates upward towards the unburned charge, compressing the end gas in the process. Similar to the single orifice case, the unburned mixture experiences autoignition with the fuel and air being consumed rapidly. However, the location and proportion of unburned mixture that is available for autoignition is quite different. The dual jets are able to consume more of the mixture before autoignition occurs, with a smaller volume experiencing autoignition. This is evident in the optical images by a clear contrast between the reacting volumes of gases exhibiting chemiluminesence, versus the burned gasses that are not emitting as much visible light. This autoignition behavior can also be observed in the pressure traces in Figure 4 where the slope of the pressure traces increases after the initial ignition event.

The ignition behavior is quite different for the non-auxiliary fueled case when there is no stratification of the fuel-air mixture between the pre-chamber and main chamber (λ=3). For the single orifice case, a colder, slower jet of gases discharge into the main chamber, entraining unburned fuel and air, and initiating combustion near the center of the combustion chamber for the single orifice nozzle. Combustion occurs throughout the jet structure, and the flame starts to propagate outward almost in a spherical manner towards the cylinder walls. The end gas near the cylinder periphery then begins to autoignite, with most of the gases in the core of the jet structure already converted to combustion products.

For the dual orifice non-auxiliary fueled case, the two jets that issue from the dual orifice are also slower, and grow into two jet plumes that compress the unburned gas and induce autoignition faster than the single orifice case. Another result seen for both non-auxiliary fueled cases is that the jets do not penetrate into the chamber as far and do not interact with the chamber walls before autoignition occurs due to the lower initial jet momentum.

The burn duration analysis gives a quantitative interpretation of the overall ignition and combustion, but does not enable the timing of the actual physics that occur to be resolved. For example, the 0-10% burn duration includes the spark discharge event, low-temperature chemical reactions that occur but do not increase the overall pressure, flame kernel propagation and convection within the pre-chamber, mass transfer from the pre-chamber contents being displaced into the main-chamber, and initial jet penetration and ignition of the main chamber charge. In the definition of the 0%-10% burn duration, the percent of the pressure rise is chosen in order to capture the ignition processes that are occurring, with the selection being somewhat arbitrary and not necessarily corresponding to any physics that are actually occurring. Ten percent is typical of this type of analysis, although in the literature one and five percent of the pressure rise are also used [34]. Similarly, the physics that occur during the 10%-90% burn duration are not able to be temporally resolved. These physics include flame propagation, jet impingement, and autoignition of the unburned mixture. Thus, a more fundamental analysis is needed to study the jet ignition process in more depth and to identify when the physics are occurring.

From Figures 3 and 4, it can be seen that there are inflection points and changes of curvature in the pressure curves. The first, second, and third derivatives of the pressure data were then taken to identify these points of interest. From the first derivative, it can determined if the pressure is rising or falling by considering if the sign is positive or negative. The change in sign of the first derivative is useful for determining when the end of compression occurs by considering the transition from a positive dP/dt to a negative value, where the pressure is no longer rising and is starting to fall. The same technique can be used to determine the end of combustion when there is no longer any significant generation of pressure due to combustion and heat transfer to the surroundings causes the pressure to decrease. Local maximums of the first derivative are also of interest as these points indicate the maximum rate of change in pressure. The second derivative is closely related to the curvature of the pressure trace. Finding the local maximum of the third derivative then gives the point where the curvature is changing the fastest. When the correct amplitude of the third derivative is chosen, it represents ignition events where the rate of pressure rise is relatively fast such as in jet ignition and autoignition. Thus, characteristic points such as the start of jet ignition in the main chamber, and onset of autoignition can be identified using the derivative curves and the times that they occur can be measured. These characteristic times with their definition and method of identification are given in Table 3.

Table 3. Definition of characteristic times and method of identification

Characteristic Time	Method of Identification
τ_0: End of compression	Transition of dP/dt from positive to negative (first occurrence)
τ_1: Beginning of jet ignition	Auxiliary Fueled: local maximum amplitude of the third derivative Non-Auxiliary Fueled: Transition of dP/dt from negative to positive
τ_2: Max rate of pressure rise due to jet ignition	Local maximum of dP/dt
τ_3: Onset of autoigntion	Local maximum amplitude of the third derivative
τ_4: Maximum rate of pressure due to autoignition	Local maximum amplitude of the first derivative
τ_5: End of combustion	Transition of dP/dt from positive to negative (second occurrence)

Figure 8 shows a pressure trace and 1st, 2nd, and 3rd derivative data for an auxiliary fueled case using PW=1.0 ms, and the dual orifice nozzle geometry. The characteristic points are superimposed onto the original pressure curve.

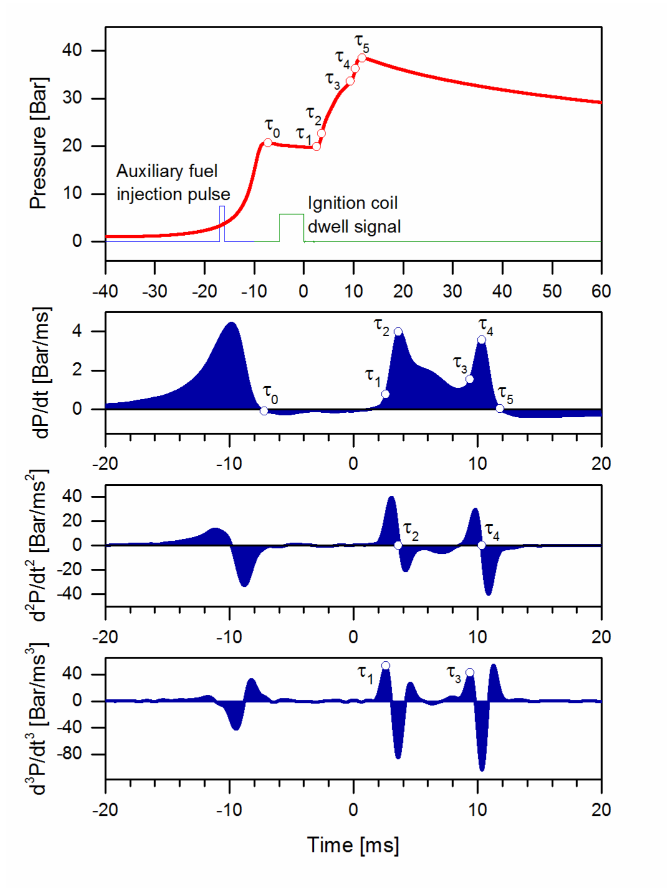

Figure 8: Pressure trace and derivative data for the dual-orifice PW=1.0 ms auxiliary fuel case

The start of jet ignition and autoignition are identified by finding the local maximum amplitude of the third derivative. Local maximums of the first derivative are also identified, which are the inflection points in the original curve. By studying the optical images, it was determined that these points define intervals in which specific combustion events are occurring. For example, the beginning of jet ignition in the main chamber occurs between the intervals defined by the start of spark discharge at 0 ms, until τ_2, which is a local maximum in the first derivative. During this interval, ignition occurs in the pre-chamber, and there is jet penetration into the main chamber. A second interval associated with jet ignition can be defined from τ_2 until τ_3, where τ_3 identifies the onset of autoignition. This jet ignition interval is characterized by wall impingement, fluid motion, and flame propagation. An autoignition interval is then defined from the onset of autoignition until the end of combustion, i.e. from τ_3 to τ_5. The optical images corresponding to these intervals for figure 8 are shown in Figure 9.

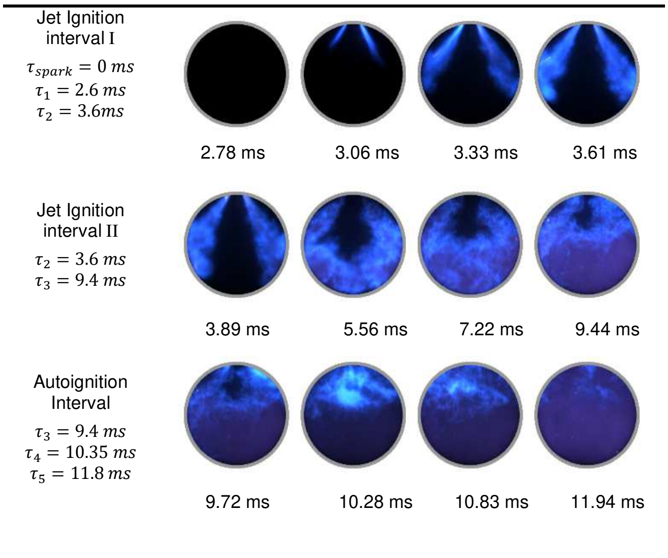

Figure 9: Optical images corresponding to characteristic time intervals for auxiliary fuel injection (dual orifice nozzle geometry, PW= 1.0 ms)

For the non-auxiliary fueled cases, the fundamental shape of the curve is different. Figure 10 gives the pressure trace and derivative data for the dual orifice, non-auxiliary fueled case. Jet ignition does not happen very quickly, and the second and third derivatives are nearly zero during the jet discharge. For this reason, the first derivative was used to determine the beginning of jet ignition. The transition from a negative dP/dt to a positive value after the spark discharge was found to identify the start of jet ignition in the main chamber.

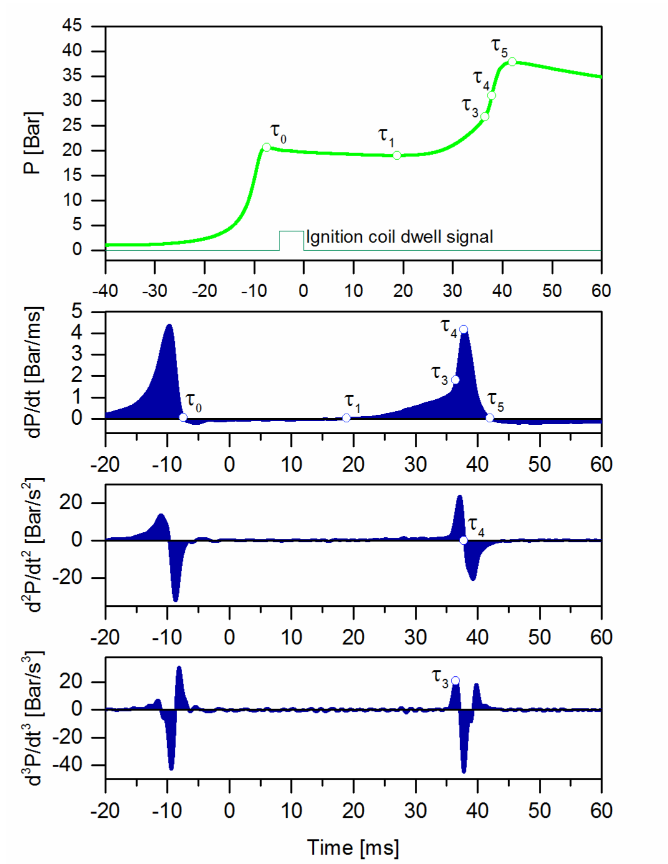

Figure 10: Pressure trace and derivative data for the dual orifice, non-auxiliary fueled case

One interesting feature of the first derivative curve for this case is that the pressure rise due to jet ignition does not reach a local maximum before the onset of autoignition. The pressure rise due to jet ignition continues to increase until the end-gas autoignition event. Thus, only two distinct intervals occur, one due to jet ignition and another due to autoignition. Figure 11 shows the optical images corresponding to these two intervals based on the pressure trace shown in Figure 10. It can be seen that the jet development and propagation is relatively slow, without much impingement onto the cylinder walls. A larger proportion of end gas is available to auto-ignite in this case.

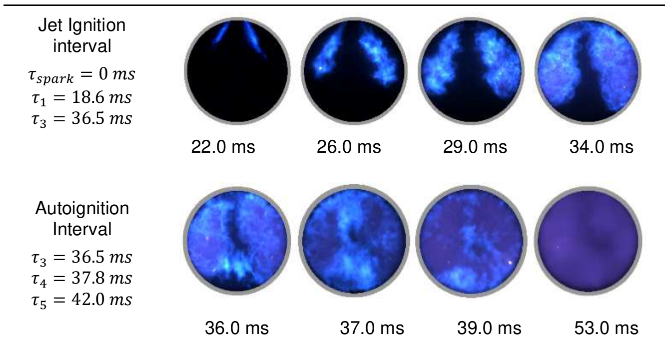

Figure 11: Optical images corresponding to characteristic time intervals for auxiliary fuel injection (dual orifice nozzle geometry, PW= 1.0 ms)

For different auxiliary fueling conditions and nozzle geometry, the pressure curves have different profiles and the characteristic points occur at different times. To compare these differences, the times were measured and plotted versus injector pulse width for both nozzles in Figure 12. The characteristic times are plotted using a logarithmic scale due to the large difference in scale between non-auxiliary fueled and fueled conditions. The mean data points are plotted and connected using a shape preserving spline, with error bands representing the standard error of the mean.

The curves for the two different nozzles have similar time scales for the non-auxiliary fueled case, with wider error bands for the dual orifice nozzle implying increased combustion instability. Similar time scales for both nozzles also occur for the 1.25 ms pulse width conditions, with small error bars implying consistent and stable combustion. This behavior agrees with the burn duration analysis previously discussed. Additional insight can be obtained by comparing the 0.75 ms pulse width case for the two nozzles. At this fuel loading condition, the dual orifice has a faster autoignition onset than the single orifice. Increasing the injector pulse width to 1.0 ms decreases the time for the onset of jet ignition for the single orifice, but does not change the onset of autoignition very much for the dual orifice. This implies that for this condition the dual jets have consumed most of the end gas in the path of the jet and increasing the fuel loading has less of an effect on the jets consuming the remaining portion of unburned fuel and air.

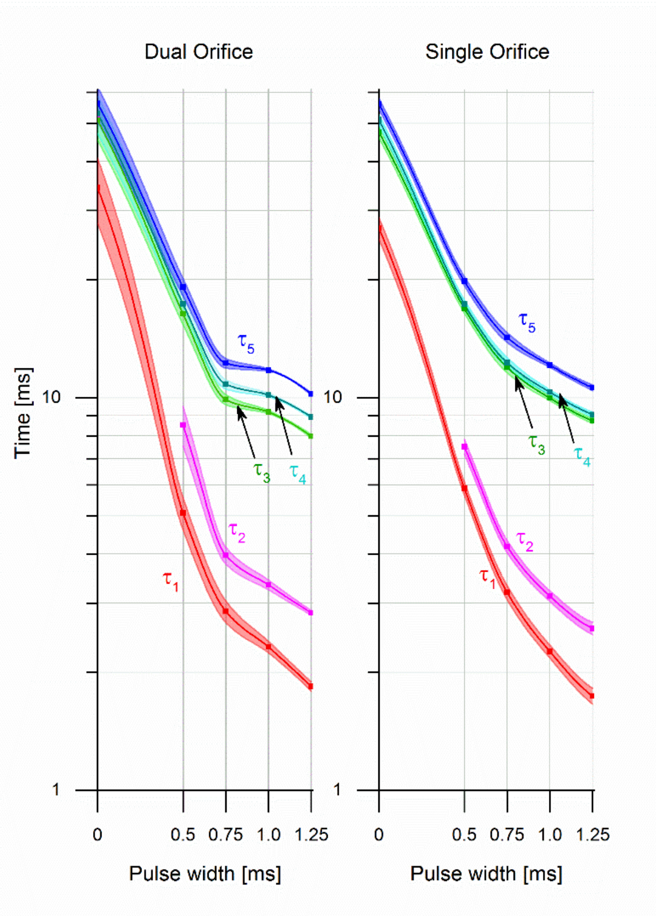

Figure 12: Characteristic time measurements as function of injector pulse width.
Error bands correspond to the standard error of the mean.

Another feature that is distinct between the two nozzle geometries is that the separation between the τ_3 and τ_4 curves are different. τ_3 represents the onset of autoignition, while τ_4 represents the maximum rate of pressure rise due to autoignition. The fact that the τ_3 and τ_4 curves occur closer together implies that the maximum pressure rise rate due to autoignition for the single orifice occurs much closer to the onset of autoignition, whereas the pressure rise rate reaches a maximum later on for the dual orifice geometry.

4. Summary and Conclusions

Experiments of TJI were performed in an optically accessible rapid compression machine using liquid iso-octane and a custom low-flow fuel injector to overcome previous limitations of using liquid fuel in the pre-chamber. The effect of nozzle geometry and auxiliary fuel injection were investigated. Jet induced autoignition behavior was also studied in depth by considering high-speed images, and pressure derivative data.

It was found that the auxiliary fuel injection was critical for combustion stability. In addition, ignition distribution via the jet being channeled through one orifice or two was important for low-auxiliary fuel loading conditions. For non-auxiliary fueling conditions, the single orifice, D=1x 3.16 mm nozzle had better ignition performance than the dual orifice D=2x 2.26 mm nozzle as evident by the pressure traces and 0%-10% burn durations. However, when the mixture stoichiometry was such that it was easily ignitable in the pre-chamber, the minimum ignition energy was reached easily and both nozzles ignited the mixture reliably. This occurred at an injector pulse width of 0.75 ms, with best performance as the injector pulse width approached 1.25 ms. Varying the orifice geometry and stoichiometry also had an effect of the jet structure and fluid mechanics. In particular, the volume of end-gas was different for the two nozzles and induced different autoignition behavior in the unburned mixture. The jet ignition and autoignition behavior was then characterized by using the pressure derivative data. Characteristic points and time intervals were identified, which corresponded to the physics that occurred as could be seen in the optical images. A time interval corresponding to jet penetration, jet impingement, and autoignition could be defined for the auxiliary fueled cases. However, only two intervals could be identified for the non-auxiliary fueled cases, one due to jet ignition and another due to autoignition of the unburned mixture. Increasing the injector pulse width was found to initiate jet ignition and autoignition faster, with little variation at injector pulse widths of 0.75, 1.00, and 1.25 ms. In summary, this paper investigated the initiation of autoignition by TJI, with the overall combustion behavior being sensitive to the fraction of auxiliary fuel injected into the pre-chamber. However, further efforts are needed to study hydrocarbon, NOx, and soot emissions for the conditions tested as this may limit the practical application in an engine.

Acknowledgements

This material is based upon work supported by The United States Department of Energy and The National Science Foundation Partnership on Advanced Combustion Engines under contract CBET-1258581.

Definitions/Abbreviations

λ	Air-Fuel Equivalence Ratio
BDC	Bottom Dead Center
EGR	Exhaust Gas Recirculation
HCCI	Homogeneous Charge Compression Ignition
JPIC	Jet Plume Injection Combustion
LAG	Avalanche Activated Combustion
LTC	Low Temperature Combustion
m_i	Injected fuel mass fraction
NO_x	Oxides of Nitrogen
RCM	Rapid Compression Machine
TDC	Top Dead Center
TJI	Turbulent Jet Ignition

References

[1] Dec JE. Advanced compression-ignition engines—understanding the in-cylinder processes. Proceedings of the Combustion Institute. 2009;32:2727-42.
[2] Olesky LM, Lavoie GA, Assanis DN, Wooldridge MS, Martz JB. The effects of diluent composition on the rates of HCCI and spark assisted compression ignition combustion. Applied Energy. 2014;124:186-98.
[3] Andwari AM, Aziz AA, Said MFM, Latiff ZA. Experimental investigation of the influence of internal and external EGR on the combustion characteristics of a controlled auto-ignition two-stroke cycle engine. Applied Energy. 2014;134:1-10.
[4] Wang X, Zhao H, Xie H. Effect of dilution strategies and direct injection ratios on stratified flame ignition (SFI) hybrid combustion in a PFI/DI gasoline engine. Applied Energy. 2016;165:801-14.
[5] Ortiz-Soto EA, Lavoie GA, Martz JB, Wooldridge MS, Assanis DN. Enhanced heat release analysis for advanced multi-mode combustion engine experiments. Applied Energy. 2014;136:465-79.
[6] Oppenheim JDDaAK. Enhanced Ignition for I.C. Engines with Premixed Gases. SAE Technical Paper 810146. 1981.
[7] Modien RM, Checkel MD, Dale JD. The Effect of Enhanced Ignition Systems on Early Flame Development in Quiescent and Turbulent Conditions. International Congress and Exposition. Detroit, Michigan: SAE International; 1991.
[8] Toulson E, Schock HJ, Attard WP. A Review of Pre-Chamber Initiated Jet Ignition Combustion Systems. SAE Technical Paper 2010-01-2263; 2010.

[9] Oppenheim AK. Prospects for Combustion in Piston Engines. SAE 2002 World Congress. Detroit, Michigan: SAE International; 2002.
[10] Oppenheim AK, Kuhl AL. Paving the Way to Controlled Combustion Engines (CCE). SAE Technical Paper 951961; 1995.
[11] Gussak LA, Karpov, V., and Tikhonov, Y. The Application of Lag-Process in Prechamber Engines. SAE Technical Paper 790692. 1979.
[12] Gussak LA, Turkish, M., and Siegla, D. High Chemical Activity of Incomplete Combustion Products and a Method of Prechamber Torch Ignition for Avalanche Activation of Combustion in Internal Combustion Engines. SAE Technical Paper 750890. 1975.
[13] Wolanski P, Oppenheim AK. Controlled Combustion Engines (CCE). SAE International; 1999.
[14] Hensinger DM, Maxson JA, Hom K, Oppenheim AK. Jet Plume Injection and Combustion. SAE Technical Paper 920414; 1992.
[15] Maxson JA, Hensinger DM, Hom K, Oppenheim AK. Performance of Multiple Stream Pulsed Jet Combustion Systems. SAE International; 1991.
[16] Maxson JA, Oppenheim AK. Pulsed jet combustion—Key to a refinement of the stratified charge concept. Symposium (International) on Combustion. 1991;23:1041-6.
[17] Murase E, Ono S, Hanada K, Oppenheim AK. Pulsed Combustion Jet Ignition in Lean Mixtures. SAE Technical Paper 942048; 1994.
[18] Murase E, Hanada K. Enhancement of Combustion by Injection of Radicals. SAE Technical Paper 2001-01-0194; 2000.
[19] Murase E, Hanada K. Control of the Start of HCCI Combustion by Pulsed Flame Jet. SAE Technical Paper 2002-01-2867; 2002.
[20] Lumsden G, Watson HC. Optimum Control of an S.I. Engine with a λ=5 Capability. SAE Technical Paper 950689; 1995.
[21] Toulson E, Watson HC, Attard WP. Gas Assisted Jet Ignition of Ultra-Lean LPG in a Spark Ignition Engine. SAE Technical Paper 2009-01-0506; 2009.
[22] Glasson N, Lumsden G, Dingli R, Watson H. Development of the HAJI System for a Multi-Cylinder Spark Ignition Engine. SAE Technical Paper 961104; 1996.
[23] Anderson EK, Attard WP, Brown A, Litke P, Grinstead K, Hoke J. Experimental Study of a Pre-Chamber Jet Igniter in a Turbocharged Rotax 914 Aircraft Engine. SAE Technical Paper 2013-01-1629; 2013.
[24] Attard WP, Parsons P. Flame Kernel Development for a Spark Initiated Pre-Chamber Combustion System Capable of High Load, High Efficiency and Near Zero NOx Emissions. SAE Int J Engines. 2010;3:408-27.
[25] Attard WP, Blaxill H. A Gasoline Fueled Pre-Chamber Jet Ignition Combustion System at Unthrottled Conditions. SAE Int J Engines. 2012;5:315-29.
[26] Attard WP, Blaxill H, Anderson EK, Litke P. Knock Limit Extension with a Gasoline Fueled Pre-Chamber Jet Igniter in a Modern Vehicle Powertrain. SAE Int J Engines. 2012;5:1201-15.
[27] Attard WP, Blaxill H. A Lean Burn Gasoline Fueled Pre-Chamber Jet Ignition Combustion System Achieving High Efficiency and Low NOx at Part Load. SAE Technical Paper 2012-01-1146; 2012.
[28] Attard WP, Blaxill H. A Single Fuel Pre-Chamber Jet Ignition Powertrain Achieving High Load, High Efficiency and Near Zero NOx Emissions. SAE Int J Engines. 2011;5:734-46.
[29] Attard WP, Toulson E, Huisjen A, Chen X, Zhu G, Schock H. Spark Ignition and Pre-Chamber Turbulent Jet Ignition Combustion Visualization. SAE Technical Paper 2012-01-0823; 2012.
[30] Toulson E, Huisjen A, Chen X, Squibb C, Zhu G, Schock H, et al. Visualization of Propane and Natural Gas Spark Ignition and Turbulent Jet Ignition Combustion. SAE Technical Paper: 2013-32-0002. SAE Int J Engines. 2012;5:1821-35.
[31] Gentz G, Thelen B, Gholamisheeri M, Litke P, Brown A, Hoke J, et al. A study of the influence of orifice diameter on a turbulent jet ignition system through combustion visualization and performance characterization in a rapid compression machine. Appl Therm Eng. 2015;81:399-411.
[32] Gentz G, Thelen B, Litke P, Hoke J, Toulson E. Combustion Visualization, Performance, and CFD Modeling of a Pre-Chamber Turbulent Jet Ignition System in a Rapid Compression Machine. SAE Int J Engines. 2015;8:538-46.
[33] Schneider CA, Rasband WS, Eliceiri KW. NIH Image to ImageJ: 25 years of image analysis. Nat Meth. 2012;9:671-5.
[34] Heywood J. Internal Combustion Engine Fundamentals: McGraw Hill; 1988.